# Effect of dual flow arrangements on the performance of mini-channel heat sink: numerical study

Hussain Ahmed Tariq[1,2] · Muhammad Anwar[2] · Hafiz Muhammad Ali[3] · Jamal Ahmed[4]

## Abstract

Water-cooled heat sinks now gained the popularity due to increased heat generation inside the microprocessor. The generated high heat flux should be removed timely and uniformly for durability of microprocessor. In this work, the thermal performance of mini-channel heat sinks for fin spacing of 0.2 mm, 0.5 mm, 1 mm and 1.5 mm is numerically investigated with various dual flow arrangements. A uniform temperature distribution is observed for all dual flow arrangements discussed in this study which was not possible using single flow inlet/outlet. A direct influence of dual flow arrangements on base temperature and pressure drop of heat sink is evaluated. The results are then compared with the conventional single flow arrangement having same dimensioned heat sink available in the literature for water as well as for $Al_2O_3$–$H_2O$ nano-fluids. The maximum drop in base temperature was noted for rectangular inlet–circular outlet duct (no gap) flow arrangement as 14.3%, 15.4%, 16.06% and 15.6% for 0.2 mm, 0.5 mm, 1 mm and 1.5 mm fin spacing, respectively, as compared to the conventional single flow arrangement using water as a cooling fluid. Rectangular inlet–circular outlet duct (no gap) was found to be the best dual flow arrangement for all fin spacing investigated. The rectangular collector was then replaced by isosceles triangular collector for the best dual flow arrangement. The maximum reduction in net mass was noted as 12.0%, using isosceles triangular collector as compared to rectangular collector with same thermal performance. Dual rectangular inlet–circular outlet (no gap) flow arrangement highlights palpable improvement in hydrothermal performance compared to the conventional single circular inlet/outlet flow arrangement along with temperature uniformity.

**Keywords** Thermal management · Mini-channel · Integral fins · Dual flow arrangement · Uniform temperature distribution

## List of symbols

| | |
|---|---|
| $A$ | Width of finned section (mm) |
| $A_{sf}$ | Surface area (mm²) |
| $A_c$ | Cross-sectional area of channel (mm) |
| $B$ | Un-finned length (mm) |
| $C_d$ | Circular duct diameter (mm) |
| $C_h$ | Circular duct height (mm) |
| $C_p$ | Specific heat capacity of water (J °C⁻¹ kg⁻¹) |
| $d_h$ | Hydraulic diameter (mm) |
| $F_p$ | Flow partition thickness (mm) |
| $F_t$ | Flow thickness (mm) |
| $g$ | Gap thickness (mm) |
| $h$ | Height of fins (mm) |
| $h_c$ | Convective heat transfer coefficient (W °C⁻¹ m⁻²) |
| $l$ | Length of fins (mm) |
| $k$ | Thermal conductivity of fluid (W m⁻¹ °C⁻¹) |
| LMTD | Log of Mean Temperature Difference (°C) |
| $\dot{m}$ | Mass flow rate (kg s⁻¹) |
| $P$ | Wetted perimeter (m) |
| Pr | Prandtl number of the fluid |
| $\Delta P$ | Pressure difference (Pa) |
| $p_t$ | Partition thickness (mm) |
| $q$ | Heat flux (W/cm²) |
| $\dot{Q}$ | Heat transfer rate (W) |
| $R_w$ | Rectangular duct width (mm) |
| $R_h$ | Rectangular duct height (mm) |
| $R_{th}$ | Thermal resistance (°C W⁻¹) |
| Re | Reynolds number of fluid |
| $s$ | Fin spacing (mm) |

✉ Hafiz Muhammad Ali
   hafiz.ali@kfupm.edu.sa

1. Department of Mechanical Engineering, Wah Engineering College, University of Wah, Wah Cantt, Pakistan

2. Department of Mechanical Engineering, Institute of Space Technology, Islamabad, Pakistan

3. Mechanical Engineering Department, King Fahd University of Petroleum and Minerals, Dhahran 31261, Saudi Arabia

4. Mechanical Department, College of Electric and Mechanical Engineering, NUST, Rawalpindi, Pakistan

| $T_b$ | Base temperature of heat sink (°C) |
| $T_o$ | Fluid outlet temperature (°C) |
| $T_i$ | Fluid inlet temperature (°C) |
| $t$ | Thickness of fins (mm) |
| $t_b$ | Thickness of heat sink base plate (mm) |
| $U_{in}$ | Inlet velocity (m s$^{-1}$) |
| $u, v, w$ | Velocity in $x$, $y$, $z$, respectively (m s$^{-1}$) |
| $\dot{V}$ | Volumetric flow rate (m$^3$ s$^{-1}$) |

**Greek symbols**

| $\lambda$ | Thermal conductivity (W m$^{-1}$ °C$^{-1}$) |
| $\mu$ | Dynamic viscosity (kg m$^{-1}$ s$^{-1}$) |
| $\rho$ | Density of fluid (kg m$^{-3}$) |

**Abbreviations**

| DCIRO | Dual circular duct inlet–rectangular duct outlet |
| DRICO | Dual rectangular duct inlet–circular duct outlet |
| DTRISRO | Dual top rectangular duct inlet–side rectangular duct outlet |
| DSRITRO | Dual side rectangular duct inlet–top rectangular duct outlet |
| ITC | Isosceles triangular collector |
| LPM | Litres per minute |
| MCHS | Mini-channel heat sink |
| SCICO | Single circular duct inlet–circular duct outlet |
| RC | Rectangular collector |

## Introduction

The performance of computers/microelectronic devices is increasing at a greater rate to meet the technological demands of today. As a consequence of this increased performance, these devices have higher heat dissipation rates. Therefore, these higher heat dissipation rates demand efficient cooling system to keep computers/microelectronic devices within safe operating temperature limits. An efficient and effective cooling system is necessary to improve the durability of these compact devices. Many contributions have been made by researchers till date aiming to develop efficient miniature heat sinks. This includes by increasing the surface area density, heat pipes, flow arrangement and/or and using the working fluid having better thermophysical properties. Xie et al. [1] numerically investigated the mini-channel heat sink using water in micro-, mini- and normal channel with single inlet/outlet flow. They found hydrothermal performance of mini-channel as the best. Jajja et al. [2] experimentally investigated the performance of mini-channel heat sink with different fin spacing including 0.2 mm, 0.5 mm, 1 mm and 1.5 mm with the conventional single inlet/outlet flow. They achieved the minimum base temperature of 40.5 °C for 0.2 mm fin spacing.

Nowadays, nano-fluids have emerged to enhance the thermal conductivity of base fluids. Ho et al. [3] experimentally investigated Al$_2$O$_3$–H$_2$O nano-fluids in micro-channel heat sink and found significant heat transfer enhancement as compared to water. Single inlet/outlet flow arrangement was used in their investigation. Manay and Sahin [4] investigated the thermal performance of micro-channel heat sink and found higher heat transfer for TiO$_2$–H$_2$O nano-fluids as compared to water with single inlet/outlet flow arrangement. Roshani et al. [5] investigated the thermal performance of pin finned heat sink using nano-fluids. They found 16% and 14% increase in heat transfer coefficients for Al$_2$O$_3$–H$_2$O and TiO$_2$–H$_2$O nano-fluids, respectively, at volumetric concentration of 2% with the conventional single inlet/outlet flow arrangement. Tariq et al. evaluated the thermal performance of cellular structure using air [6], water [7], Al$_2$O$_3$–H$_2$O and CuO–H$_2$O nano-fluids [8] as a coolant. They found the least base temperature for Al$_2$O$_3$–H$_2$O followed by CuO–H$_2$O, water and air. The conventional single inlet/outlet flow arrangement was used in their investigation. Rafati et al. [9] experimentally investigated the silica, alumina and titania nanoparticles in base fluids for thermal management of the mini-channels. They found the highest drop of processor temperature from 49.4 to 43.9 using 1% volumetric concentration alumina nano-fluids. Saeed et al. evaluated the thermal hydraulic performance of mini-channel heat sinks using water [10] and Al$_2$O$_3$–H$_2$O nano-fluids [11]. The geometry under their investigation was integral finned heat sink (fin spacing of 0.2 mm, 0.5 mm, 1 mm and 1.5 mm) with the conventional single inlet/outlet flow arrangement. They found significant drop in base temperature using nano-fluids as compared to water. Anwar et al. [12] numerically investigated the thermal performance of mini-channel heat sinks using CuO–H$_2$O nano-fluids. A significant thermal performance as compared to water was found with the conventional single inlet/outlet flow arrangement. Various studies reported the hydrothermal performance of miniature heat sinks with the conventional single inlet/outlet flow arrangement [13–15]. Neyestani et al. [16] investigated inline, staggered and porous heat sinks where porous leads to significant thermal enhancement. Wang et al. [17] numerically investigated the interrupted heat sink with different rib shapes (rectangle, triangle and trapezoid). They found best overall heat transfer performance for trapezoid ribs. Arasteh et al. [18] enhanced the hydrothermal performance of porous double-layer sinusoidal heat sink. Sajid et al. [19] investigated the thermal performance of wavy channel heat sink using TiO2 water-based nano-fluids as a coolant with the conventional single inlet/outlet flow. Soudagar et al. [20] presented various studies on thermal analysis of mini-channel heat sink. A lot of recent studies showed the potential of using nano-fluids due to increased thermophysical properties [21–25]. Recent progressions of magnetic nanoparticles

have attained the attention of many researchers due to their attractive properties. Various studies were performed to analyse magneto-hydrodynamic Jeffrey nano-material fluid flow induced by curved stretchable sheet to examine heat transfer characteristics [26, 27]. Different studies investigate the Darcy–Forchheimer nano-liquid flow with Arrhenius activation energy [28–30]. Bhatti et al. [31] and Prakash et al. [32] investigated the effects of heat and mass transfer on magnetized suspended nanoparticles. Prakash et al. [33] investigated the nano-fluids flow in tapered porous channel.

One of the important features of good thermal management miniature devices is flow distribution inside these devices. Various flow arrangements have been investigated by researchers for effective cooling. Chein and Chen [34] numerically investigated the performance of heat sinks using various single inlet/outlet flow arrangements including I type, N type, S type, D type, U type and V type. They concluded the performance of V-type flow arrangement to be the best among all the investigated arrangements on the basis of overall heat transfer coefficient, thermal resistance and pressure drop. Kumar and Singh [35] proposed numerical study for non-uniform temperature distribution at the base of mini-channel heat sink. They investigated four different channel arrangements including I type, Z type, C type and N type with single inlet/outlet flow. Uniform flow was found for C type in mini-channel, while better temperature uniformity was found for I-type arrangement. Mu et al. [36] performed numerical study to improve the temperature uniformity of heat sink. They investigated three types of channel head configuration including U-type, Z-type and circular turning and found circular turning to be the best one. Kumaran et al. [37] performed experimental and numerical study to investigate the effects of flow distribution in inlet/outlet configuration and header design. They found best flow distribution for C-type arrangement as compared to I type, V type, Z type and U type. They also found that triangle-shaped header provides better flow distributions as compared to trapezoidal and rectangular one. Sehgal et al. [38] experimentally investigated the effect of U-type, P-type and S-type flow arrangements to evaluate the performance of micro-channel heat sink. They found the minimum friction factor for P-type and maximum Nusselt number for U-type flow arrangement. Toghraie et al. [39] numerically investigated the effect of flow and heat transfer in smooth, sinusoidal and zigzag-shaped micro-channel. They found zigzag-shaped channel as the best one among the others. Hadipour et al. [40] investigated the effect of micro-pin on flow and heat transfer of a circular impinging jet. They found increase in Nusselt number and heat transfer for a row of micro-pin around the impingement point on the target plate. Hosseinalipour et al. [41] numerically investigated the thermal performance of steady and pulsating impinging jet in porous block. Zunaid et al. [42] performed numerical study on rectangular and

semi-cylindrical micro-channel heat sink with single inlet/outlet flow and found semi-cylindrical heat sink to be the best as compared to rectangular heat sink. Effat et al. [43] numerically investigated the effect of single-, double- and triple-layer micro-channel heat sink along the parallel and counter flow arrangements on thermal performance. They found better surface uniformity for counter flow as compared to parallel flow. Moreover, increasing number of layer results in the reduction in the base surface temperature. Shen et al. [44] numerically investigated the straight and staggered double layer with parallel and counter flow arrangements. They found the thermal performance of staggered double-layer micro-channel with counter flow to be the best. Hao et al. [45] numerically investigated the flow uniformity and heat transfer capacity of a U-shaped heat sink based on orthogonal experiment design with single inlet/outlet flow. Miry et al. [46] investigated the thermal performance of miniature tangential heat sink with circular channel. They found heat transfer coefficient of water in tangential flow arrangement to be 131% more as compared to the conventional flow arrangement heat sink. Dharaiya et al. [47] performed numerical study to investigate uniform flow distribution in plate fin heat exchanger. They found a uniform flow through channels for tapered header as compared to circular. Gan et al. [48] investigated the micro-channel with impinging jets and side outlets. They found better heat transfer and fluid flow with the addition of side outlets. Akbari et al. [49] investigated the horizontal and straight fluid passage to examine the effect on flow and heat transfer. They found performance of straight passage better than that of horizontal passage. Tran et al. [50] numerically investigated five different channel shapes, i.e. circle, square, trapezium, two concave surfaces and two convex surfaces. The thermal performance of circular channel was found to be the best as compared to others. They also performed a test with multi-nozzle and concluded that multi-nozzle micro-channel could considerably reduce the thermal resistance.

A lot of contributions have been made by researchers including flow arrangements for effective thermal management in miniature devices. It is evident from the literature survey that flow distribution inside miniature devices plays a vital role in thermal management. In this study, the conventional single circular duct inlet–circular duct outlet (SCICO) is replaced by novel dual flow arrangements. A uniform temperature distribution was achieved at the base by all dual flow arrangements discussed in this study. None of the above studies has addressed the integral finned mini-channel channel heat sink (MCHS) with dual flow arrangements to achieve temperature uniformity of heat sink which is the prime focus of present work. MCHS was divided into two equal portions each with a separate flow arrangement. The results evaluated were then compared with the conventional SCICO having same heat sinks dimensions at same heating

power of 325 W present in the literature. Furthermore, the hydrothermal performance of the best flow arrangement with rectangular collector (RC) was compared with isosceles triangular collector (ITC).

## Numerical model

ANSYS 16.0 commercial software was used to solve conservation equations from (1–5). Pressure-based solver with absolute velocity formulation was used. Transport equation for Realizable k-ε model was used for the present study. Pressure and velocity coupling was controlled by Semi-Implicit Method for Pressure-Linked Equations (SIMPLE). A second-order spatial discretization scheme was used for the pressure, while for the discretization of momentum, turbulent kinetic energy and turbulent dissipation rate second-order upwind scheme was used. Outlet was considered at 0 gauge pressure. A constant heat of 325 W was supplied at the bottom chip of heat sink. The velocities in solid region were zero everywhere ensured by a numerical solution algorithm for the conjugated problem [51, 52]. The following assumptions [1, 8, 11] were made during the modelling of the numerical solutions.

1. Flow is considered steady and incompressible.
2. No heat generation inside the heat sink and no viscous heating.
3. Radiation heat transfer is neglected.
4. Thermal properties are considered to be constant throughout the flow.

Governing Eqs. (1 to 5) [1] on the basis of above assumptions were as follows for conservation of mass, momentum, energy, turbulence kinetic energy and turbulence dissipation rate:

Conservation of mass

$$\frac{\partial}{\partial x_i}\left(\rho u_i\right) = 0 \tag{1}$$

Conservation of momentum

$$\frac{\partial}{\partial x_i}\left(\rho u_i u_j\right) = -\frac{\partial p}{\partial x_j} + \frac{\partial}{\partial x_i}\left[\left(\mu + \mu_t\right)\frac{\partial \mu_j}{\partial x_i}\right] + \frac{\partial}{\partial x_i}\left[\left(\mu + \mu_t\right)\frac{\partial \mu_i}{\partial x_j}\right],$$
$$j = 1, 2, 3 \tag{2}$$

Conservation of energy

$$\frac{\partial}{\partial x_i}\left(\rho u_i T\right) = \frac{\partial}{\partial x_i}\left[\left(\frac{\lambda}{c_p} + \frac{\mu_t}{\sigma_T}\right)\frac{\partial T}{\partial x_i}\right] \tag{3}$$

Conservation of turbulence kinetic energy ($k$)

$$\frac{\partial}{\partial x_i}\left(\rho k u_i\right) = \frac{\partial}{\partial x_i}\left[\left(\mu + \frac{\mu_t}{\sigma_k}\right)\frac{\partial k}{\partial x_i}\right] + G_k - \rho\varepsilon \tag{4}$$

Conservation of turbulence dissipation rate ($\varepsilon$)

$$\frac{\partial}{\partial x_i}\left(\rho\varepsilon u_i\right) = \frac{\partial}{\partial x_i}\left[\left(\mu + \frac{\mu_t}{\sigma_\varepsilon}\right)\frac{\partial \varepsilon}{\partial x_i}\right] + \rho C_1 S\varepsilon - \rho C_2 \frac{\varepsilon^2}{k + \sqrt{v\varepsilon}} \tag{5}$$

where $G_k$ is generation of turbulence kinetic energy which can be defined as

$$G_k = -\rho\overline{u_i' u_j'}\frac{\partial u_j}{\partial x_i} \tag{6}$$

$\mu_t$ is turbulent viscosity and is defined as

$$\mu_t = \frac{\rho C_\mu k^2}{\varepsilon} \tag{7}$$

$C_\mu$ is defined as

$$C_\mu = 1 / \left[A_o + \left(\frac{A_s k U^*}{\varepsilon}\right)\right] \tag{8}$$

$A_s$ is defined as

$$A_s = \sqrt{6}\cos\emptyset \tag{9}$$

where $C_2 = 1.9$, $\sigma_k = 1$, $\sigma_\varepsilon = 1.2$, $A_o = 4.04$ are constants.

The following boundary conditions were imposed for this study as:

1. No-slip velocity boundary condition at the solid walls.
2. The uniform inlet velocity entering in the heat sink is shown in Eq. (10).

   at $\quad y = F_t + t_b + C_h, u = 0, v = U_{in}, w = 0 \tag{10}$

3. Inside the solid region, the velocity is considered to be zero everywhere as shown in Eq. (11).

   at solid regions, $\quad u = 0, v = 0, w = 0 \tag{11}$

4. Heat flux is supplied at the bottom of the heat sink as shown in Eq. (12).

   at $y = 0, -\lambda\frac{\partial T}{\partial y} = q \tag{12}$

5. The right, left and top surfaces of the heat sink are considered to be adiabatic as shown from Eqs. (13–15).

   at $x = 0, \frac{\partial T}{\partial x} = 0 \tag{13}$

   at $x = A, \frac{\partial T}{\partial x} = 0 \tag{14}$

$$y = F_t + t_b, \quad \frac{\partial T}{\partial y} = 0 \tag{15}$$

## Mesh sensitivity analysis

To ensure independency of solution from the mesh, a mesh study was performed on a selective dual rectangular duct inlet–circular duct outlet (DRICO) with 0.5 mm spacing. Five cases with different numbers of elements ranging from 2 million to 4 million were analysed. The solution was considered to be independent of the mesh when the relative temperature difference $(T_b - T_i)$ found less than 0.5%. It was observed that after 3.5 million numbers of elements, influence of mesh on the solution was less than 0.5% as shown in Fig. 1. Based on this comparison, the number of elements with case 4 was selected for the whole study to save computational time and memory. The iteration is considered converged when the relative deviation between two consecutive iterations is found less than the specified small value $\varepsilon_\emptyset$, which was set $10^{-7}$ in present investigation [1]. $\emptyset$ represent variables $u$, $v$, $w$, $k$ and $\varepsilon$.

$$\max\left(\left|\emptyset_{i,j,k}^n - \emptyset_{i,j,k}^{n-1}\right| \middle/ \left|\emptyset_{i,j,k}^n\right|\right) < \varepsilon_\emptyset \tag{16}$$

To validate the numerical results, Nusselt number computed numerically was compared with Colburn correlation given in Eq. (17) [53] for the best flow arrangement DRICO (no gap). Numerically computed Nusselt number and Nusselt number calculated from correlation with volumetric flow rate were found very close to each as shown in Fig. 2. Both the curves were in good agreement with a maximum difference of not more than 8%.
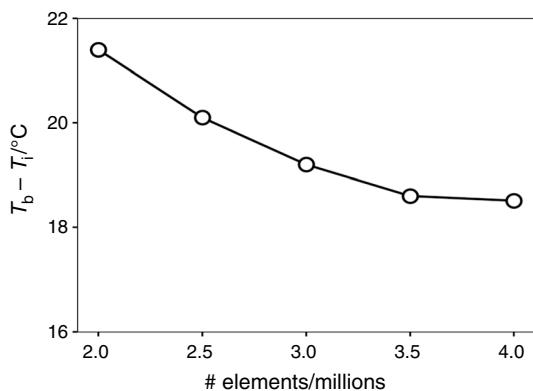
$$Nu = 0.023 Re^{0.8} Pr^{1/3} \tag{17}$$

## Data reduction

To evaluate the data, the following procedure was adopted. Heat transfer rate is calculated from Eq. (18) [14]

$$\dot{Q} = \dot{m} C_p (T_o - T_i) \tag{18}$$

LMTD is calculated from Eq. (19) [14]

$$LMTD = \frac{(T_b - T_i) - (T_b - T_o)}{\ln\left(\frac{(T_b - T_i)}{(T_b - T_o)}\right)} \tag{19}$$

Convective heat transfer coefficient is calculated from Eq. (20) [14]

$$h_c = \dot{m} \frac{C_p (T_o - T_i)}{A_{sf} LMTD} \tag{20}$$

Thermal resistance is calculated from Eq. (21) [2]

$$R_{th} = LMTD / \dot{Q} \tag{21}$$

Hydraulic diameter can be calculated from Eq. (22) [14]

$$d_h = 4 A_c / P \tag{22}$$

Nusselt number can be calculated from Eq. (23) [14]

$$Nu = h_c \frac{d_h}{k} \tag{23}$$

Reynolds number can be calculated from Eq. (24) [14]
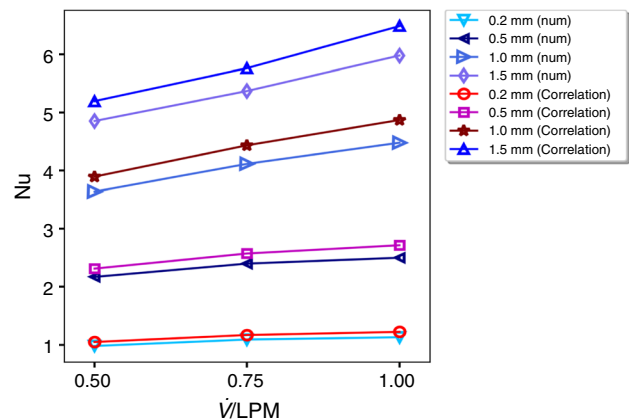
$$Re = \frac{\rho U_{in} d_h}{\mu} \tag{24}$$



Fig. 1 Mesh sensitivity analysis



Fig. 2 Nusselt number with volumetric flow rate

## Heat sink description

Heat sinks were modelled on ANSYS design modular to desire dimensions as shown in Table 1. Four different integral fin spacing (0.2 mm, 0.5 mm, 1 mm and 1.5 mm) heat sinks were used for present investigation. All the other parameters of MCHS were kept constant. Heat sinks were parted in two equal parts. A square chip of 28.7 mm * 28.7 mm with 0.5 mm thickness was placed exactly at the centre of MCHS to provide a constant heat flux at the base. Physical description of the investigated MCHS is shown in Fig. 3.

## Flow description

Heat sink was divided in two equal portions. Each portion was provided a separate flow passage. Four different dual flow passages were investigated on four different integral fin spacing (0.2 mm, 0.5 mm, 1 mm and 1.5 mm) MCHSs. The details of flow arrangements and cases solved are given in Table 2. Pictorial view of all flow arrangements discussed in this study is shown in Fig. 4. All flow arrangements were solved with respective gap and no gap cases. In gap arrangement, flow will

**Table 1** Dimensions of MCHS

| $l$ | $A$ | $B$ | $h$ | $t$ | $t_b$ | $p_t$ | $g$ | $C_h$ | $C_d$ | $R_h$ |
|---|---|---|---|---|---|---|---|---|---|---|
| 22 | 55 | 10 | 3 | 1 | 3 | 1 | 0.5 | 7 | 7 | 7 |
| $F_t$ | | $s$ | | | | | | $R_w$ | $F_p$ | |
| 3 (no gap) | 3.5 (gap) | 0.2 | 0.5 | 1 | 1.5 | | | 2 | 1 | |
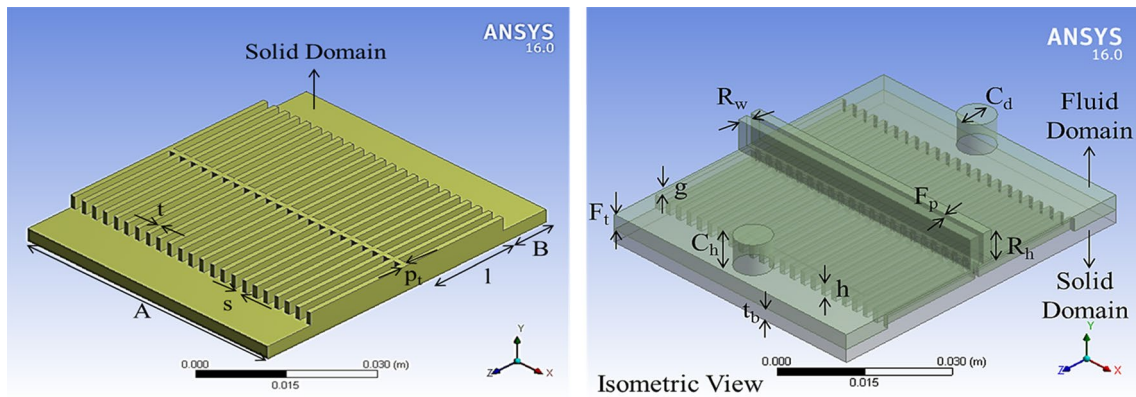


**Fig. 3** Physical model of heat sink

**Table 2** Details of flow arrangement and numerical cases solved

| Flow arrangement | Description | Case | Fin spacing |
|---|---|---|---|
| DCIRO | Dual circular duct inlet–rectangular duct outlet | Gap | 0.2 mm, 0.5 mm, 1 mm, 1.5 mm |
| | | No gap | 0.2 mm, 0.5 mm, 1 mm, 1.5 mm |
| DRICO | Dual rectangular duct inlet–circular duct outlet | Gap | 0.2 mm, 0.5 mm, 1 mm, 1.5 mm |
| | | No gap | 0.2 mm, 0.5 mm, 1 mm, 1.5 mm |
| DTRISRO | Dual top rectangular duct inlet–side rectangular duct outlet | Gap | 0.2 mm, 0.5 mm, 1 mm, 1.5 mm |
| | | No gap | 0.2 mm, 0.5 mm, 1 mm, 1.5 mm |
| DSRITRO | Dual side rectangular duct inlet–top rectangular duct outlet | Gap | 0.2 mm, 0.5 mm, 1 mm, 1.5 mm |
| | | No gap | 0.2 mm, 0.5 mm, 1 mm, 1.5 mm |
| ITC DRICO | Isosceles triangular collector dual rectangular duct inlet–circular duct outlet | No gap | 0.2 mm, 0.5 mm, 1 mm, 1.5 mm |
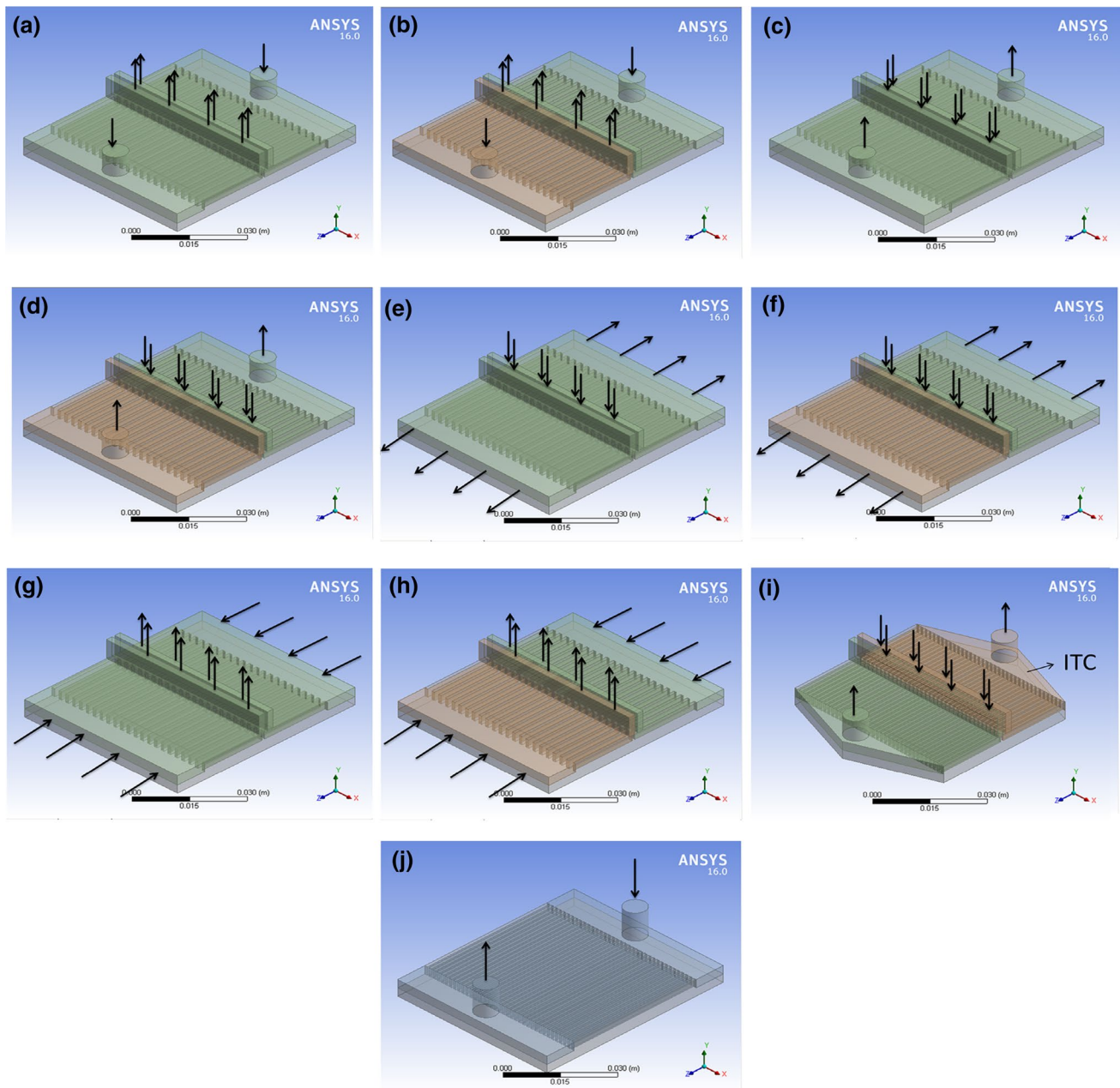
**Fig. 4** Flow arrangements: **a** DCIRO (gap), **b** DCIRO (no gap), **c** DRICO (gap), **d** DRICO (no gap), **e** DTRISRO (gap), **f** DTRISRO (no gap), **g** DSRITRO (gap), **h** DSRITRO (no gap), **i** ITC DRICO (no gap) and **j** SCICO [10–12]

be present between the fins as well as on the upper surface of fins, whereas in no gap case the flow will remain between the fins only. A detailed comparison of dual flow arrangements with the conventional flow arrangement SCICO is provided in "Results and discussion" section.

## Results and discussion

Performance of MCHS with 0.2 mm, 0.5 mm, 1 mm and 1.5 mm integral fin spacing using dual flow configuration for each case is discussed in detail in this section. A comprehensive comparison is provided with the conventional

single flow configuration reported in the literature for same dimensioned MCHS. Results are also compared with the water-based $Al_2O_3$ nano-fluids present in the literature for same dimensioned MCHS. The best flow arrangement is further investigated with the ITC and the hydrothermal performance is compared.

## 2 mm fin spacing MCHS

### Base temperature

Base temperature noted at the chip (placed at the bottom) for all flow arrangements with overall volumetric flow rate for 0.2 mm fin spacing is shown in Fig. 5. It was observed that base temperature of gap arrangement was high for 0.2 mm fin spacing MCHS. Gap above the fins provides a void passage to flow which was not suitable in small fin spacing like
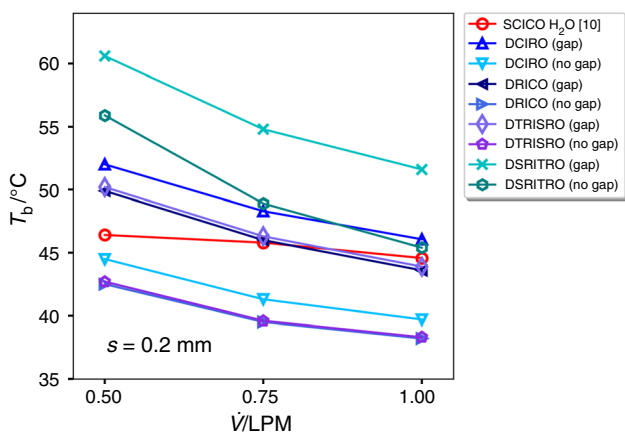


**Fig. 5** Base temperature with volumetric flow rate
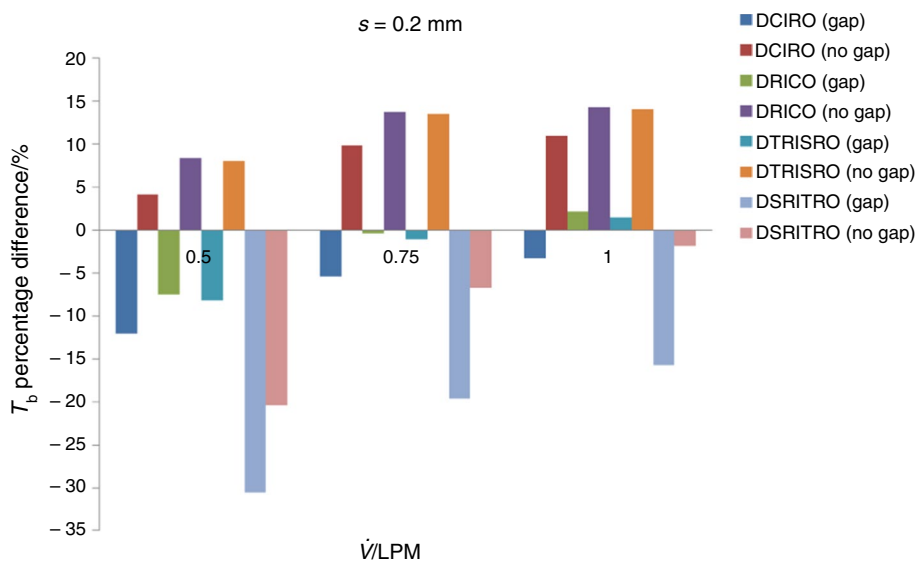
0.2 mm. Base temperature decreases with increasing flow rate for all flow arrangements. The reason of this decrease is due to the increase in the mass flow rate by increasing volumetric flow rate which results in increased heat transfer. The minimum base temperature was noted for DRICO (no gap) and DTRISRO (no gap) flow arrangement as 38.2 °C and 38.3 °C, respectively, at 1 LPM. the base temperature noted at 1 LPM was 44.6 °C using the conventional SCICO flow arrangement [10]. The reason of least recorded base temperature value for DRICO (no gap) and DTRISRO (no gap) as compared to all other flow arrangements was the better flow dispersion inside the heat sink. Flow enters from the top rectangular duct and provides a better flow passage between the integral fins. Base temperature noted for DRICO (no gap), DTRISRO (no gap) and DCIRO (no gap) was below than that of the conventional SCICO at all flow rates.

Percentage difference in base temperature for dual flow arrangements compared to the conventional SCICO flow arrangement [10] is shown in Fig. 6. The values above 0 show percentage increment, while the values below 0 show decrement as compared to SCICO. DRICO (no gap) flow arrangement was found to be the best one for 0.2 mm fin spacing at all flow rates. The percentage reduction in base temperature noted for DRICO (no gap) was 8.42%, 13.75% and 14.31% at 0.5 LPM, 0.75 LPM and 1 LPM, respectively, as compared to SCICO.

### Pressure drop

Pressure drop with volumetric flow rate across the MCHS is presented in Fig. 7. Pressure drop increases with increasing volumetric flow rate. At higher volumetric flow rates, mass flow of fluid inside the channel increases which results in higher pressure drop. Pressure drop for all flow arrangement
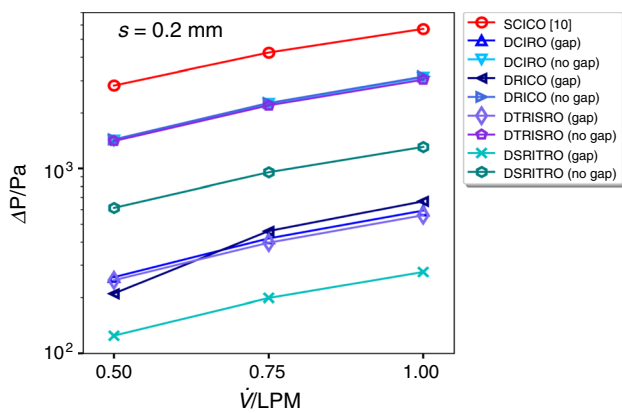
**Fig. 6** Base temperature percentage difference with volumetric flow rate

**Fig. 7** Pressure drop with volumetric flow rate



**Fig. 8** Base temperature with volumetric flow rate

cases was found lower than that of the reported conventional [10] SCICO values at all flow rates. Pressure drop noted for DRICO (no gap), DCIRO (no gap) and DTRISRO (no gap) was approximately close to each other. Lowest pressure drop was noted for DSRITRO (gap) 124.5 Pa, 198.6 Pa and 274.8 Pa at 0.5 LPM, 0.75 LPM and 1 LPM, respectively. The reason was the easy passage flow of lowest pressure drop. Highest pressure drop was noted for DRICO (no gap) as 1436.6 Pa, 2262.6 Pa and 3147.4 Pa at 0.5 LPM, 0.75 LPM and 1 LPM, respectively. Flow outlet from a small cylindrical duct results in higher pressure drop. A significant difference was observed for all flow arrangements with respective gap and no gap cases in small fin spacing like 0.2 mm. Whole fluid passed through small fin spacing in no gap cases which was the reason of the increase in pressure drop for no gap cases.

## 0.5 mm fin spacing MCHS

### Base temperature

Base temperature noted for all flow arrangements with overall volumetric flow rate for 0.5 mm fin spacing is shown in Fig. 8. A significant base temperature reduction was found for all flow arrangements as compared to the conventional SCICO [10] except DSRITRO (gap) and DSRITRO (no gap) at all flow rates. The minimum base temperature was noted for DRICO (no gap) and DTRISRO (no gap) flow arrangement at all flow rates as compared to other flow arrangements. Flow enters from the top rectangular duct and provides a better flow passage between the integral fins which is the reason of least recorded values of base temperature for DRICO (no gap) and DTRISRO (no gap). The minimum temperature noted for DRICO (no gap) and DTRISRO (no gap) was 40.1 °C and 40.3 °C, respectively, at 1 LPM. It was also noted that the base temperature of gap and no gap cases with respective flow arrangement was close to each
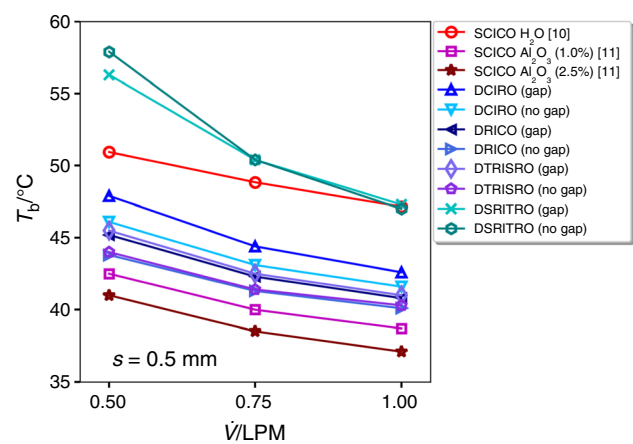
other; however, no gap was recommended. Gap above the fins provides a void passage to flow which did not affect significantly in small fin spacing like 0.5 mm. The base temperature for DRICO (no gap) and DTRISRO (no gap) was found close to water-based $Al_2O_3$ nano-fluids with 1% volumetric concentration [11]. At all flow rates, base temperature using $Al_2O_3$ nano-fluids was found the least as compared to all flow arrangements.

Percentage difference in base temperature for dual flow arrangements compared to the conventional single flow arrangement [10] is shown in Fig. 9. DRICO (no gap) was found to be the best flow arrangement for 0.5 mm fin spacing. The reduction in base temperature percentage difference noted for DRICO (no gap) was 14.01%, 15.43% and 14.95% at 0.5 LPM, 0.75 LPM and 1 LPM, respectively, as compared to SCICO. A very small percentage base temperature difference was observed for the gap and no gap cases for all flow arrangements except DSRITRO. The results were also compared with the water-based $Al_2O_3$ nano-fluids [11] having volumetric concentration of 1% and 2.5%. There was a significant difference found for nano-fluids at all flow rates.

### Pressure drop

Pressure drop with volumetric flow rate across the MCHS is presented in Fig. 10. Pressure drop increases with increasing volumetric flow rate. Pressure drop for all flow arrangement cases was found lower than that of the reported conventional SCICO [10] values at all flow rates. A significant difference was observed for all flow arrangements with respective gap and no gap cases except DSRITRO. The lowest pressured drop was noted for DSRITRO (gap) as 50.6 Pa, 80.1 Pa and 111.5 Pa at 0.5 LPM, 0.75 LPM and 1 LPM, respectively, due to easy passage flow. The highest pressure drop was noted for DRICO (no gap) 230.74 Pa, 390.2 Pa and 575.7 Pa

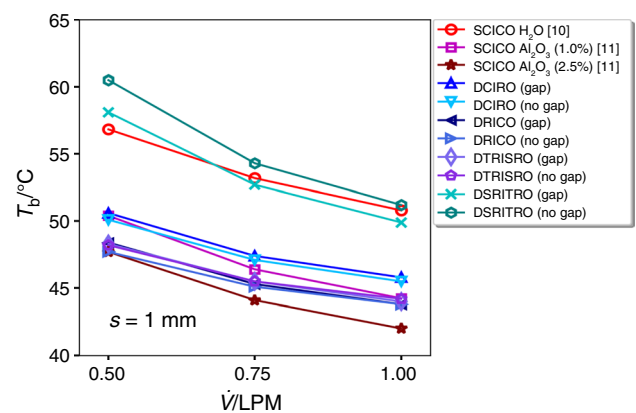**Fig. 9** Base temperature percentage difference with volumetric flow rate



**Fig. 10** Pressure drop with volumetric flow rate
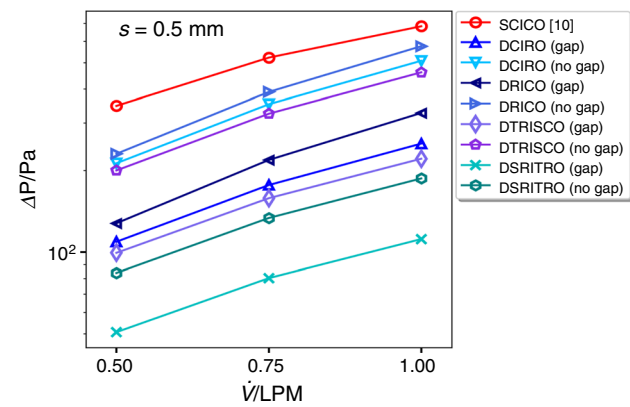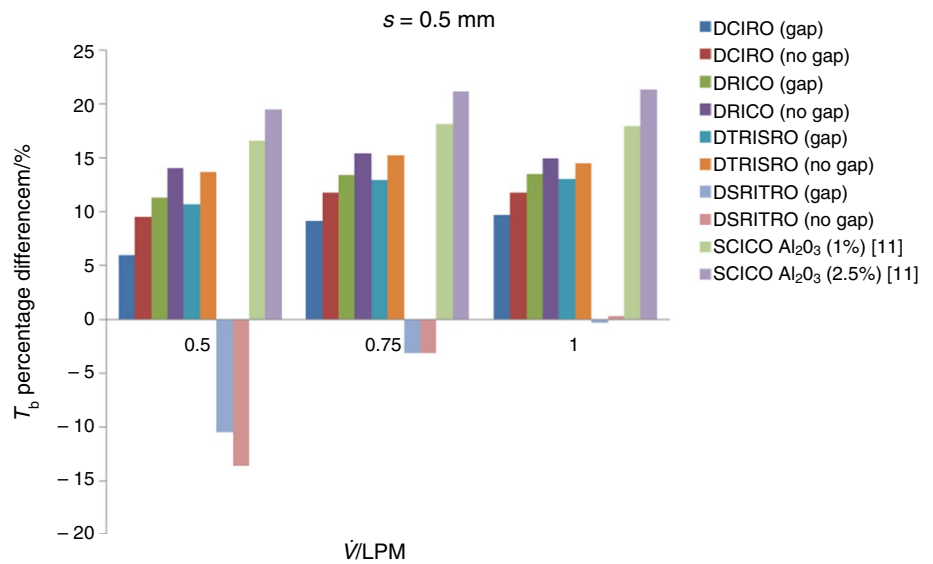


**Fig. 11** Base temperature with volumetric flow rate



at 0.5 LPM, 0.75 LPM and 1 LPM, respectively, due to flow outlet from a small cylindrical duct.

## 1 mm fin spacing MCHS

### Base temperature

Base temperature noted for all flow arrangements with overall volumetric flow rate for 1 mm fin spacing is shown in Fig. 11. A significant drop in base temperature was noted for all flow arrangements as compared to the conventional SCICO [10] except DSRITRO (no gap) and DSRITRO (gap). It was observed that gap and no gap cases for respective flow arrangements did not significantly affect the results except DSRITRO (no gap) and DSRITRO (gap). Gap above the fins provides a void passage to flow which favours significantly in comparatively large fin spacing like 1 mm in DSRITRO. As the fin spacing was large enough for fluid to

flow, the gap above the fins goes in favour of large fin spacing. The minimum base temperature was found for DRICO (no gap) as 43.8 °C at 1 LPM. Flow enters from the top rectangular duct and provides a better flow passage between the integral fins which is the reason of least recorded values of base temperature for DRICO (no gap). It was observed that base temperature reduces using DRICO and DTRISRO with both gap and no gap cases when compared with water-based $Al_2O_3$ nano-fluids with 1% volumetric concentration [11] at 0.5 LPM and 0.75 LPM. The base temperature noted at 1 LPM was very close to each other. Base temperature was found very close at 0.5 LPM for DTRISRO (gap and no gap) and DRICO (gap and no gap) as compared to water-based $Al_2O_3$ nano-fluids [11] with 2.5% volumetric concentration.

Percentage difference in base temperature for dual flow arrangements compared to the conventional single flow arrangement [10] is shown in Fig. 12. DRICO (no gap) was found to be the best flow arrangement for 1 mm fin

**Fig. 12** Base temperature percentage difference with volumetric flow rate
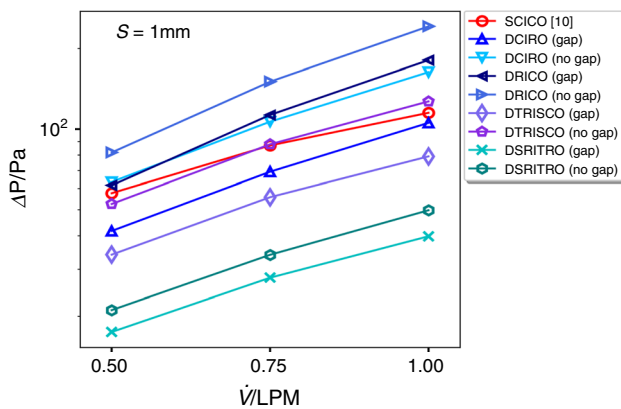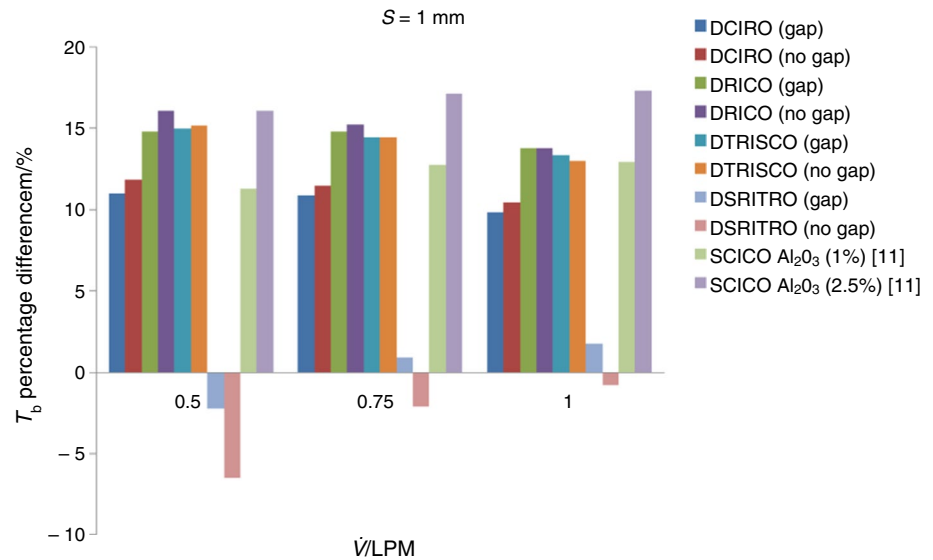


**Fig. 13** Pressure difference with volumetric flow rate

spacing. The reduction in base temperature percentage difference noted for DRICO (no gap) was 16.06%, 15.20% and 13.77% at 0.5 LPM, 0.75 LPM and 1 LPM, respectively, as compared to SCICO. DRICO (no gap) outclassed the water-based $Al_2O_3$ nano-fluids with 1% concentration [11] at all flow rates. At lower flow rates, DRICO (no gap) base temperature was found equally to water-based $Al_2O_3$ nano-fluids with 2.5% concentration [11], while a small difference was noticed at higher flow rates.

### Pressure drop

Pressure drop with volumetric flow rate across the MCHS is presented in Fig. 13. Pressure drop increases with increasing volumetric flow rate. It was noted that at lower flow rates, pressure drop variation among all cases was low as compared to variations at higher flow rate. The maximum pressure drop was noted 81.7 Pa, 150.3 Pa and 241.5 Pa at

0.5 LPM, 0.75 LPM and 1 LPM, respectively, for DRICO (no gap) due to flow outlet from a small cylindrical duct. The minimum pressure drop was noted 17.4 Pa, 27.8 Pa and 39.7 Pa at 0.5 LPM, 0.75 LPM and 1 LPM, respectively, for DSRITRO (gap) due to easy flow passage. Pressure drop noted for DCIRO (no gap) and DRICO (gap) was approximately found close to each other. The noted value of pressure drop for DCIRO (gap), DTRISRO (gap) and DSRITRO (gap and no gap) was found below than that of the conventional SCICO [10]. Pressure drop noted for DTRISRO (no gap) was almost same compared to the conventional SCICO. A significant difference was observed for flow arrangements with respective gap and no gap cases except DSRITRO.

### 1.5 mm fin spacing MCHS

#### Base temperature

Base temperature noted for all flow arrangements with overall volumetric flow rate for 1.5 mm fin spacing is shown in Fig. 14. A significant drop in base temperature was noted for all flow arrangements as compared to the conventional SCICO except DSRITRO (no gap) and DSRITRO (gap). It was observed that gap and no gap cases for DSRITRO and DTRISRO flow arrangements significantly affect the results, while DCIRO and DRICO were not affected by this. Gap above the fins provides a void passage to flow which favours significantly in comparatively large fin spacing like 1.5 mm in DSRITRO and DTRISRO. As the fin spacing was large enough for fluid to flow, the gap above the fins goes in favour of large fin spacing. The minimum base temperature was noted for DRICO (gap) and DRICO (no gap) as 45.5 °C and 45.7 °C, respectively. Flow enters from the top rectangular duct and provides a better flow passage between the integral
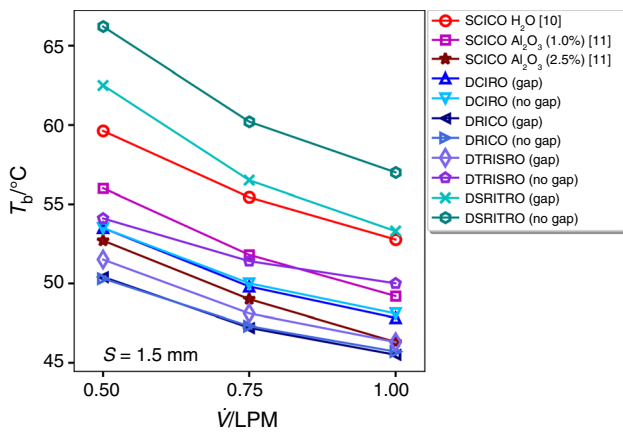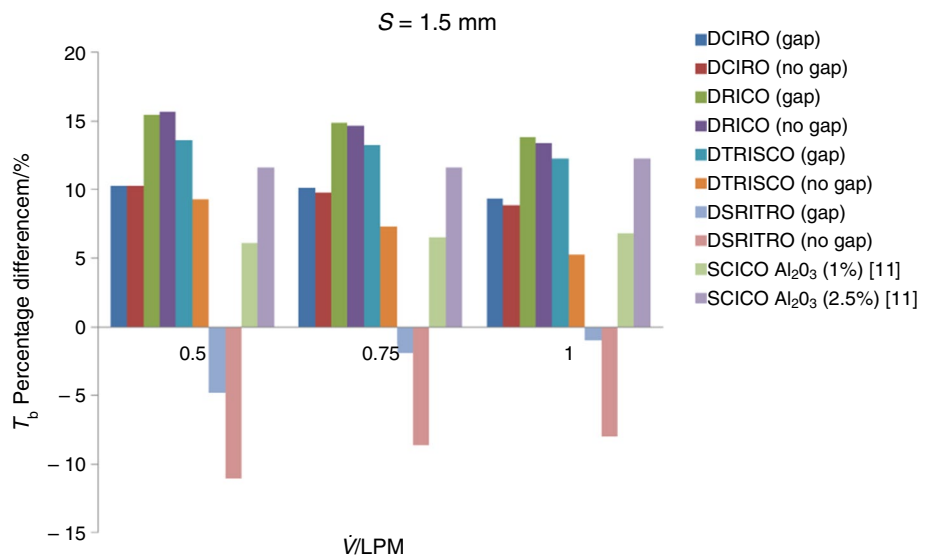
Fig. 14 Base temperature with volumetric flow rate

## Pressure drop

Pressure drop with volumetric flow rate across the MCHS is presented in Fig. 16. Pressure drop increases with increasing volumetric flow rate. Pressure drop for DCIRO (gap) and DTRISRO (gap and no gap) was found approximately equal to the conventional SCICO [10] at all flow rates. The highest pressure drop was noted for DRICO (no gap) as 58.6 Pa, 115.2 Pa and 191.2 Pa at 0.5 LPM, 0.75 LPM and 1 LPM, respectively, due to flow outlet from a small cylindrical duct. Difference in pressure drop for all flow arrangement was observed between respective gap and no gap cases except DSRITRO. For large fin spacing like 1.5 mm, no significant difference in pressure drop was observed. Lowest pressure drop was observed
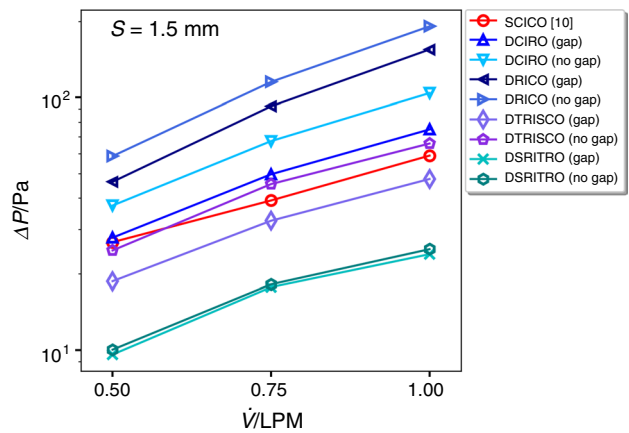
fins which is the reason of least recorded values of base temperature for DRICO. The base temperature noted for DRICO (gap and no gap) completely outclasses water-based $Al_2O_3$ nano-fluids [11] with volumetric concentrations of 2.5% at all flow rates.

Percentage difference in base temperature for dual flow arrangements compared to the conventional single flow arrangement [10] is shown in Fig. 15. DRICO (gap) and DRICO (no gap) were found to be the best flow arrangement for 1.5 mm fin spacing. The reduction in base temperature percentage difference noted for DRICO (gap) was 15.46%, 14.84% and 13.77% and for DRICO (no gap) was 15.63%, 14.66% and 13.39% at 0.5 LPM, 0.75 LPM and 1 LPM, respectively, as compared to SCICO. DRICO (gap) and DRICO (no gap) completely outclass the base temperature of water-based $Al_2O_3$ nano-fluids with 1% and 2.5% concentration at all flow rates.



Fig. 16 Pressure difference with volumetric flow rate



Fig. 15 Base temperature percentage difference with volumetric flow rate

for DSRITRO (gap) as 9.6 Pa, 17.7 Pa and 23.9 Pa at 0.5 LPM, 0.75 LPM and 1 LPM, respectively, due to easy passage flow.

## Temperature Uniformity

Temperature uniformity in electronic devices is essential for durability and longer operation. All the flow arrangements investigated in this study are able to achieve uniform temperature distribution inside the heat sink. Base temperature contour at base of MCHS for dual flow arrangements with fin spacing of 0.5 mm is shown in Fig. 17. This temperature uniformity was not possible using conventionally SCICO arrangement as shown in Fig. 17j.

## Isosceles triangular collector

The best of all flow arrangements was DRICO (no gap) among all integral fin spacing as discussed in "Results and discussion" section. The rectangular collector (RC) was used for all of these flow arrangements. The rectangular collector was then replaced by the isosceles triangular

collector (ITC) for DRICO (no gap) flow arrangement, and the results were then compared.

## Base temperature

Base temperature noted values for ITC and RC were found very close to each other as shown in Fig. 18. The base temperature percentage reduction noted for ITC as compared RC was found not more than 1% for all integral fin spacing cases at all flow rates. However, a significant reduction in base temperature can be seen as compared to noted values in the literature with the conventional SCICO flow arrangement with respective fin spacing as shown in Fig. 18. It is evident from the results that base temperature was found minimum for small fin spacing as compared to higher fin spacing. Small fin spacing provides higher surface area which results in higher heat transfer rate. The least base temperature was observed for 0.2 mm fin spacing due to higher surface area as compared to others.
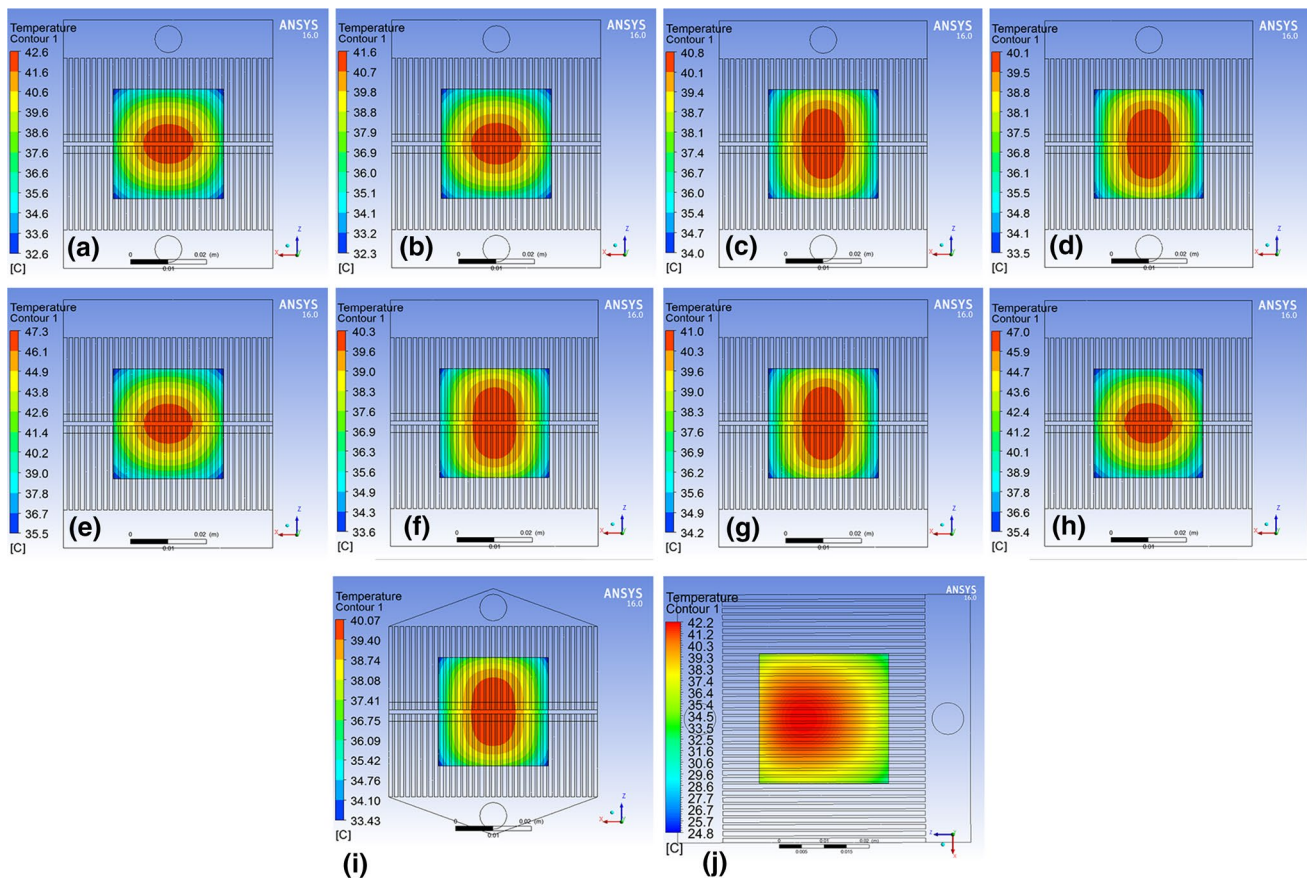


**Fig. 17** Temperature distribution at base: **a** DCIRO (gap), **b** DCIRO (no gap), **c** DRICO (gap), **d** DRICO (no gap), **e** DSRITRO (gap), **f** DSRITRO (no gap), **g** DTRISRO (gap), **h** DTRISRO (no gap), **i** ITC DRICO (no gap) and **j** SCICO [12]
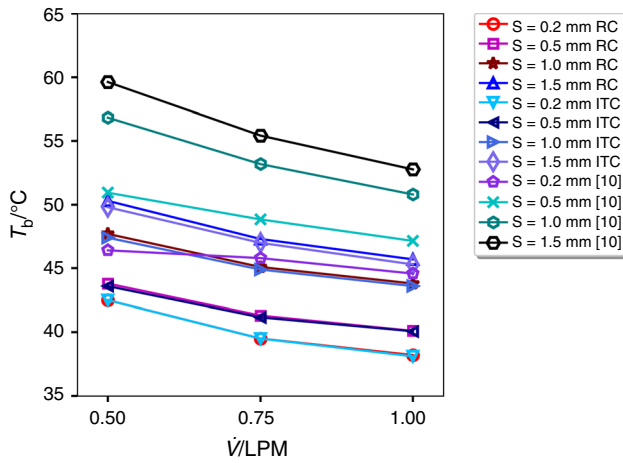
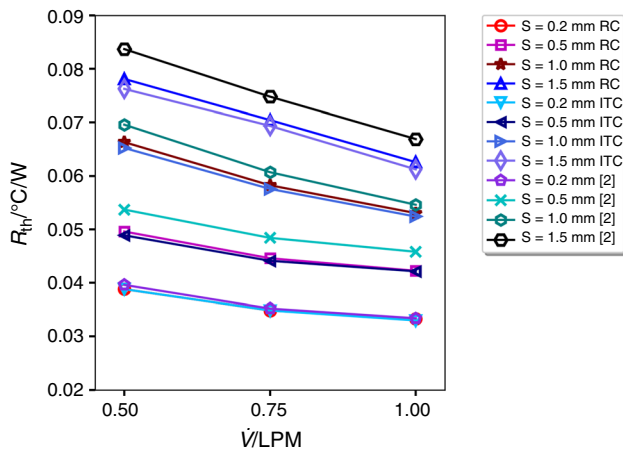**Fig. 18** Base temperature of DRICO (no gap) flow arrangement

**Table 3** Percentage difference in $R_{th}$ for DRICO (no gap) ITC and SCICO RC

|  | $s = 0.2$ mm/% | $s = 0.5$ mm/% | $s = 1$ mm/% | $s = 1.5$ mm/% |
|---|---|---|---|---|
| 0.5 LPM | 2.0 | 9.0 | 6.3 | 8.9 |
| 0.75 LPM | 1.0 | 8.9 | 5.2 | 7.3 |
| 0.5 LPM | 1.2 | 8.0 | 4.0 | 8.5 |
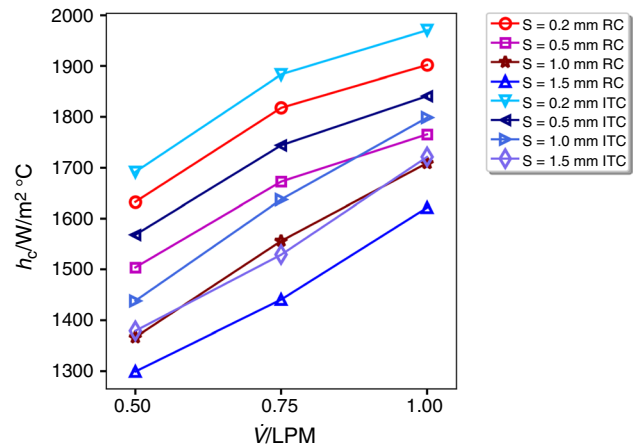


**Fig. 20** Convective heat transfer coefficient of DRICO (no gap) flow arrangement



**Fig. 19** Thermal resistance of DRICO (no gap) flow arrangement

### Thermal resistance

Thermal resistance of DRICO (no gap) flow arrangement with volumetric flow rate is shown in Fig. 19. Thermal resistance is inversely related to heat transfer rate. Lower thermal resistance value depicts the greater amount of heat transfer, while higher value depicts lower heat transfer. Lower thermal resistance value ensures the minimum resistance for heat to transfer. Thermal resistance of 0.2 mm fin spacing was noted as the least followed by 0.5 mm, 1 mm and 1.5 mm fin spacing as shown in Fig. 19. The minimum thermal resistance was noted as 0.033 °C/W for 0.2 mm fin spacing at 1 LPM with ITC. The maximum thermal resistance was noted as 0.076 °C/W for 1.5 mm fin spacing at 0.5 LPM with ITC. A minute difference was found between RC and ITC. The percentage difference between the RC and ITC was estimated not more than 2.3% for any fin spacing. The percentage reduction in thermal resistance for DRICO (no

gap) flow arrangement with ITC as compared to reported value for the conventional SCICO with RC is given in detail in Table 3.

### Convective heat transfer coefficient

Convective heat transfer coefficient with volumetric flow rate is shown in Fig. 20. Maximum value of convective heat transfer coefficient was noted for 0.2 mm fin spacing as 1691.6 W/$^0$C m$^2$. The values noted for 0.2 mm fin spacing were the highest followed by 0.5 mm, 1 mm and 1.5 mm fin spacing. The values computed for DRICO (no gap) flow arrangement with RC and ITC for their respective fin spacing cases were found very close to each other. Percentage difference between DRICO (no gap) RC and ITC was noted not more than 6.1% among all fin spacing.

### Pressure drop

Pressure drop of DRICO (no gap) with ITC and RC arrangement is shown in Fig. 21. Pressure drop increases with increasing volumetric flow rate. It was noted that RC and ITC values were found very close to each other. The maximum difference of less than 15% was noted between RC and ITC. Maximum pressure drop was noted for 0.2 mm
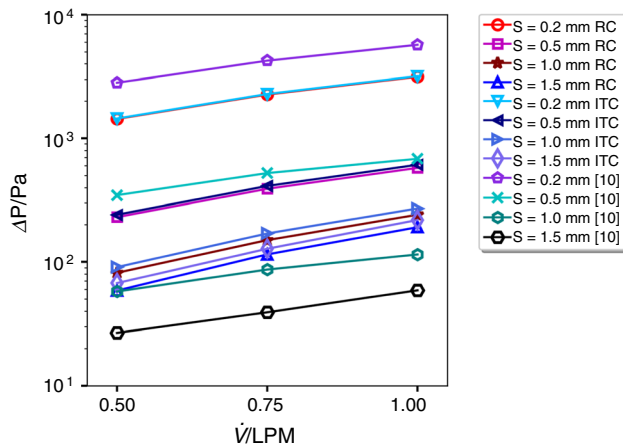
**Fig. 21** Pressure drop of DRICO (no gap) flow arrangement
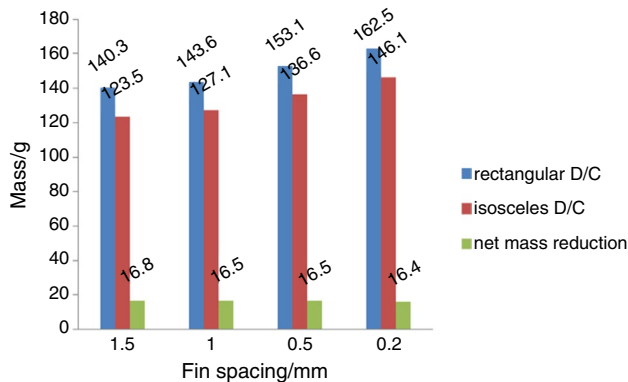


**Fig. 22** Net mass reduction

fin spacing (ITC) as 3180 Pa, while the minimum pressure drop was noted for 1.5 mm fin spacing (RC) as 58.6 Pa. It is evident from results that pressure drop increases with decreasing fin spacing. The reason is that the frontal blockage area increases for small fin spacing due to the addition of a number of fins per unit area as compared to larger fin spacing which results in higher pressure drop.

### Net mass reduction

It is discussed in detail in Sect. 3.6 that hydrothermal performance of DRICO (no gap) flow arrangement with ITC and RC arrangement was found very close to each other. However, net mass was reduced as 16.8 g, 16.5 g, 16.5 g and 16.4 g for 1.5 mm, 1 mm, 0.5 mm and 0.2 mm fin spacing, respectively. Net mass reduction (mass fluid + mass solid) noted for DRICO (no gap) flow arrangement with ITC as compared to RC is given in Fig. 22. The percentage reduction in net mass was noted as 12.0%, 11.5%, 10.8% and 10.1% for 1.5 mm, 1 mm, 0.5 mm and 0.2 mm fin spacing, respectively.

## Conclusions

The hydrothermal performance of mini-channel heat sinks with various dual flow arrangements having integral fin spacing of 0.2 mm, 0.5 mm, 1 mm and 1.5 mm was numerically investigated. The core findings of the present investigation are:

- For 0.2 mm and 0.5 mm fin spacing, the minimum base temperature was noted for DTRISRO (no gap) and DRICO (no gap) flow arrangements. For 1 mm fin spacing, the base temperature for DRICO (gap and no gap) and DTRISRO (gap and no gap) flow arrangements was the minimum. For 1.5 mm fin spacing, the minimum base temperature was noted for DRICO (gap and no gap) flow arrangements.
- For 0.2 mm fin spacing, it was observed that base temperature was high, while pressure drop was low for gap arrangement as compared to no gap arrangement using. For 0.5 mm fin spacing, a minute difference in base temperature was observed between gap and no gap arrangements; however, pressure drop was high for no gap as compared to gap arrangement. For 1 mm fin spacing, no significant difference was found in temperature drop for gap and no gap arrangement, while pressure drop was observed higher for no gap as compared to gap arrangement. For 1.5 mm fin spacing, no significant difference in base temperature was found for gap and no gap arrangement except for DTRISRO. Pressure drop of no gap arrangement was observed high as compared to gap arrangement except DSRITRO.
- For 0.2 mm, 0.5 mm and 1 mm fin spacing, minimum pressure drop was noted for DSRITRO (gap) flow arrangement. For 1.5 mm fin spacing, the minimum pressure drop was noted for DSRITRO (gap and no gap) flow arrangement.
- A uniform temperature distribution was observed for all dual flow arrangements discussed in the present investigation.
- For 1 mm fin spacing, at lower flow rates, base temperature for DRICO (no gap) flow arrangement was found equal to water-based $Al_2O_3$ nano-fluids with 2.5% concentration, while a small difference was noticed at higher flow rates. The base temperature was found lower for DRICO (no gap) flow arrangement compared to 1% concentration of water-based $Al_2O_3$ nano-fluids. For 1.5 mm fin spacing, DRICO (gap) and DRICO (no gap) flow arrangements completely outclass the base temperature of water-based $Al_2O_3$ nano-fluids with 1% and 2.5% concentration at all flow rates.

- DRICO (no gap) flow arrangement highlights palpable improvement compared to the conventional SCICO flow arrangement.
- The collector of best flow arrangement was then replaced by isosceles triangular collector. The maximum percentage reduction in net mass of DRICO (no gap) flow arrangement was noted as 12.0%, using isosceles triangular collector as compared to rectangular collector with same thermal hydrothermal performance.

# References

1. Tran N, Chang Y, Teng J, Greif R. A study on five different channel shapes using a novel scheme for meshing and a structure of a multi-nozzle microchannel heat sink. Int J Heat Mass Transf. 2017;105:429–42.
2. Akbari O, Khodabandeh E, Kahbandeh F, Toghraie D, Khalili M. Numerical investigation of heat transfer of nanofluid flow through a microchannel with heat sinks and sinusoidal cavities by using novel nozzle structure. J Therm Anal Calorim. 2019;138:737–52.
3. Ali H, Babar H, Shah T, Sajid M, Qasim M, Javed S. Preparation techniques of $TiO_2$ nanofluids and challenges: a review. Appl Sci. 2018;8(4):587.
4. Ali M, Shoukat A, Tariq H, Anwar M, Ali H. Header design optimization of mini-channel heat sinks using $CuO–H_2O$ and $Al_2O_3–H_2O$ nanofluids for thermal management. Arab J Sci Eng. 2019;44(12):10327–38.
5. Anwar M, Tariq H, Shoukat A, Ali H, Ali H. Numerical study for heat transfer enhancement using $CuO–H_2O$ nano-fluids through minichannel heat sinks for microprocessor cooling. J Therm Sci. 2019. https://doi.org/10.2298/TSCI180722022A.
6. Arasteh H, Mashayekhi R, Goodarzi M, Motaharpour S, Dahari M, Toghraie D. Heat and fluid flow analysis of metal foam embedded in a double-layered sinusoidal heat sink under local thermal non-equilibrium condition using nanofluid. J Therm Anal Calorim. 2019;138:1461–76.
7. Asma M, Othman W, Muhammad T. Numerical study for Darcy–Forchheimer flow of nanofluid due to a rotating disk with binary chemical reaction and Arrhenius activation energy. Mathematics. 2019;10(7):921.
8. Bhatti M, Zeeshan A, Tripathi D, Ellahi R. Thermally developed peristaltic propulsion of magnetic solid particles in biorheological fluids. Indian J Phys. 2018;92:423–30.
9. Chein R, Chen J. Numerical study of the inlet/outlet arrangement effect on microchannel heat sink performance. Int J Therm Sci. 2009;48:1627–38.
10. Dharaiya V, Radhakrishnan A, Kandlikar S. Evaluation of a tapered header configuration to reduce flow maldistribution in minichannels and microchannels. In: Proceedings of the ASME 2009 7th international conference on nanochannels, microchannels and minichannels. Pohang, South Korea; 2009.
11. Effat M, AbdelKarim M, Hassan O, Abdelgawad M. Numerical investigations of the effect of flow arrangement and number of layers on the performance of multi-layer microchannel heat sinks. In: Proceedings of the ASME 2015 international mechanical engineering congress and exposition. Houston, Texas; 2016.
12. Gan T, Ming T, Fang W, Liu Y, Miao L, Ren K, et al. Heat transfer enhancement of a microchannel heat sink with the combination of impinging jets, dimples, and side outlets. J Therm Anal Calorim. 2019. https://doi.org/10.1007/s10973-019-08754-z.
13. Hadipour A, Zargarabadi M, Dehghan M. Effect of micro-pin characteristics on flow and heat transfer by a circular jet impinging to the flat surface. J Therm Anal Calorim. 2020. https://doi.org/10.1007/s10973-019-09232-2.
14. Hamza B, Usman S, Ali H. Viscosity of hybrid nanofluids: a critical review. Therm Sci. 2019;23(3):1713–54.
15. Hao X, Wu Z, Chen X, Xie G. Numerical analysis and optimization on flow distribution and heat transfer of a U-type parallel channel heat sink. Adv Mech Eng. 2014;7(2):672451.
16. Hayat T, Saif R, Ellahi R, Muhammad T, Alsaedi A. Simultaneous effects of melting heat and internal heat generation in stagnation point flow of Jeffrey fluid towards a nonlinear stretching surface with variable thickness. Int J Therm Sci. 2018;132:344–54.
17. Ho CJ, Wei LC, Li ZW. An experimental investigation of forced convective cooling performance of a microchannel heat sink with $Al_2O_3$/water nanofluid. Appl Therm Eng. 2010;30(2–3):96–103.
18. Hosseinalipou S, Rashidzadeh S, Moghimi M, Esmailpour K. Numerical study of laminar pulsed impinging jet on the metallic foam blocks using the local thermal non-equilibrium model. J Therm Anal Calorim. 2020. https://doi.org/10.1007/s10973-019-09225-1.
19. Jajja SA, Ali W, Ali HM, Ali AM. Water cooled minichannel heat sinks for microprocessor cooling: effect of fin spacing. Appl Therm Eng. 2014;64:76–82.
20. Kumar S, Singh P. A novel approach to manage temperature non-uniformity in minichannel heat sink by using intentional flow maldistribution. Appl Therm Eng. 2019;163:114403.
21. Kumaran R, Kumaraguruparan G, Sornakumar T. Experimental and numerical studies of header design and inlet/outlet configurations on flow mal-distribution in parallel micro-channels. Appl Therm Eng. 2013;58:205–16.
22. Manay E, Sahin B. Heat transfer and pressure drop of nanofluids in a microchannel heat sink. Heat Transf Eng. 2016;38(5):510–22.
23. Miry S, Roshani M, Hanafizadeh P, Ashjaee M, Amini F. Heat transfer and hydrodynamic performance analysis of a miniature tangential heat sink using $Al_2O_3–H_2O$ and $TiO_2–H_2O$ nanofluids. Exp Heat Transf. 2016;29(4):536–60.
24. Mu Y, Chen L, He Y, Tao W. Numerical study on temperature uniformity in a novel mini-channel heat sink with different flow field configurations. Int J Heat Mass Transf. 2015;85:147–57.
25. Muhammad T, Lu D, Mahanthesh B, Eid M, Ramzan M, Dar A. Significance of Darcy–Forchheimer porous medium in nanofluid through carbon nanotubes. Commun Theor Phys. 2018;70:361. https://doi.org/10.1088/0253-6102/70/3/361.
26. Neyestani M, Nazari M, Shahmardan M, Sharifpur M, Ashouri M, Meye J. Thermal characteristics of CPU cooling by using a novel porous heat sink and nanofluids. J Therm Anal Calorim. 2019;138:805–17.
27. Patankar S. Numerical heat transfer and fluid flow. New York: Hemisphere; 1980.
28. Prakash J, Siva E, Tripathi D, Kuharat S, Anwar Bég O. Peristaltic pumping of magnetic nanofluids with thermal radiation and temperature-dependent viscosity effects: modelling a solar magneto-biomimetic nanopump. Renew Energy. 2019;133:1308–26.
29. Prakash J, Tripathi D, Tiwari A, Sait S, Ellahi R. Peristaltic pumping of nanofluids through a tapered channel in a porous environment: applications in blood flow. Symmetry. 2019;11(7):868.
30. Qiu T, Wen D, Hong W, Liu Y. Heat transfer performance of a porous copper micro-channel heat sink. J Therm Anal Calorim. 2020;139:1453–62.
31. Rafati M, Hamidi AA, Niaser MS. Applications of nanofluids in computer cooling systems (heat transfer performance of nanofluids). Appl Therm Eng. 2012;45:9–14.
32. Rohsenow W, Hartnett W. Handbook of heat transfer. New York: McGraw-Hill; 1973.

33. Roshani M, Miry S, Hanafizadeh P, Ashjaee M. Hydrodynamics and heat transfer characteristics of a miniature plate pin-fin heat sink utilizing $Al_2O_3$–water and $TiO_2$–water nanofluids. J Therm Sci Eng Appl. 2015;7(3):031007-1.

34. Saeed M, Kim M. Heat transfer enhancement using nanofluids ($Al_2O_3$–$H_2O$) in mini-channel heatsinks. Int J Heat Mass Transf. 2018;120:671–82.

35. Saeed M, Kim M. Numerical study on thermal hydraulic performance of water cooled mini-channel heat sinks. Int J Refrig. 2016;69:147–64.

36. Saif R, Hayat T, Ellahi R, Muhammad T, Alsaedi A. Darcy–Forchheimer flow of nanofluid due to a curved stretching surface. Int J Numer Methods Heat Fluid Flow. 2019;29(1):2–20.

37. Saif R, Muhammad T, Sadia H, Ellahi R. Hydromagnetic flow of Jeffrey nanofluid due to a curved stretching surface. Phys A Stat Mech Appl. 2020. https://doi.org/10.1016/j.physa.2019.124060.

38. Sajid M, Ali H. Recent advances in application of nanofluids in heat transfer devices: a critical review. Renew Sustain Energy Rev. 2019;103:556–92.

39. Sajid M, Ali H. Thermal conductivity of hybrid nanofluids: a critical review. Int J Heat Mass Transf. 2018;126:211–34.

40. Sajid M, Ali H, Sufyan A, Rashid D, Zahid S, Rehman W. Experimental investigation of $TiO_2$–water nanofluid flow and heat transfer inside wavy mini-channel heat sinks. J Therm Anal Calorim. 2019;137:1279–94.

41. Sehgal S, Murugesan K, Mohapatra S. Experimental investigation of the effect of flow arrangements on the performance of a micro-channel heat sink. Exp Heat Transf. 2011;24:215–33.

42. Shen H, Zhang Y, Yan H, Sunden B, Xie G. Convective heat transfer of parallel-flow and counter-flow double-layer microchannel heat sinks in staggered arrangement. In: Proceedings of the ASME 2017 international mechanical engineering congress and exposition. Tampa, Florida; 2018.

43. Soudagar M, Kalam M, Sajid M, Afzal A, Banapurmath N, Akram N, et al. Thermal analyses of minichannels and use of mathematical and numerical models. Numer Heat Transf Part A Appl. 2020;77(5):497–537.

44. Tao W. Numerical heat transfer. 2nd ed. Xi'an: Xi'an Jiaotong University Press; 2001.

45. Tariq HA, Shoukat AA, Anwar M, Israr A, Ali HM. Water cooled micro-hole cellular structure as a heat dissipation media: an experimental and numerical study. J Therm Sci. 2018. https://doi.org/10.2298/TSCI180219184T.

46. Tariq H, Anwar M, Malik A. Numerical investigations of mini-channel heat sink for microprocessor cooling: effect of slab thickness. Arab J Sci Eng. 2020. https://doi.org/10.1007/s13369-020-04370-4.

47. Tariq H, Israr A, Khan Y, Anwar M. Numerical and experimental study of cellular structures as a heat dissipation media. Heat Mass Transf. 2019;55(2):501–11.

48. Tariq H, Shoukat A, Hassan M, Anwar M. Thermal management of microelectronic devices using micro-hole cellular structure and nanofluids. J Therm Anal Calorim. 2019;136(5):2171–82.

49. Toghraie D, Abdollah M, Pourfattah F, Akbari O, Ruhani B. Numerical investigation of flow and heat transfer characteristics in smooth, sinusoidal and zigzag-shaped microchannel with and without nanofluid. J Therm Anal Calorim. 2018;131:1757–66.

50. Wahab A, Hassan A, Qasim M, Ali H, Babar H, Sajid M. Solar energy systems—potential of nanofluids. J Mol Liq. 2019;289:111049.

51. Wang W, Li Y, Zhang Y, Li B, Sundén B. Analysis of laminar flow and heat transfer in an interrupted microchannel heat sink with different shaped ribs. J Therm Anal Calorim. 2019. https://doi.org/10.1007/s10973-019-09156-x.

52. Xie XL, Tao WQ, He YL. Numerical study of turbulent heat transfer and pressure drop characteristics in water-cooled minichannel heat sink. J Electron Packag. 2007;129:247–55.

53. Zunaid M, Jindal A, Gakhar D, Sinha A. Numerical study of pressure drop and heat transfer in a straight rectangular and semi cylindrical projections microchannel heat sink. J Therm Eng. 2017;3(5):1453–65.